Finite Element Analysis of Nonlinear Silicon Micro Cantilever-Polymer Systems

Undergraduate Honors Thesis

Presented in Partial Fulfillment of the Requirements for Graduation with Distinction in the Department of Mechanical Engineering at The Ohio State University

Junfeng Li

Mechanical and Aerospace Engineering Department

Micro/Nano Multi-physical Dynamics Lab

The Ohio State University

Committee

Advisor: Dr. Hanna Cho

Committee Member: Dr. Rebecca Dupaix

Abstract

Micro-electro-mechanical systems (MEMS) have been known for their phenomenal performance in sensing, controlling, and actuating. Researchers and engineers have widely investigated MEMS for various applications such as hypersensitive sensors, radio frequency (RF) MEMS, optical MEMS, signal processing elements, and logic devices. Micromechanical resonators are often used in MEMS as a main mechanical component in aforementioned applications and the functionality of MEMS largely depends on the dynamic behavior of micro-resonators. Due to their small size and low damping, nonlinearities are readily observed in the dynamic response of micro-resonators. Recent research efforts are focusing on exploiting unique nonlinear features in designing tunable nonlinear micro-resonators. This research aims to take advantage of finite element analysis (FEA) as a complementary approach to experimental characterization and analytical modeling in designing nonlinear micro-systems. As well as providing an accurate estimation of the level of nonlinearity in the device, FEA provides various detailed field outputs at any location of the structure during nonlinear resonances. The proposed FEA methodology is based on imposing an initial deflection to the structure at the corresponding mode shape and releasing it from a relatively large amplitude to have the structure experience the free decay response. Backbone curves and frequency content graphs (including fast Fourier and wavelet transform) are obtained after postprocessing the dynamic response. FEA is conducted for two types of structures including single and double silicon micro-cantilevers with nonlinear polymer couplings. The simulated backbone curves have shown good agreement with experimental results for both types of structures. FEA is also employed to obtain design criteria to calculate the targeted level of nonlinearity. In a single cantilever-polymer system, the effect of material properties of the nonlinear coupling on the backbone curve are studied parametrically to

prove that there is a threshold value for Young's modulus of polymer which switches the global dynamics from nonlinear hardening to softening. In a double cantilever-polymer system, the physical position and thickness of the polymer coupling are found to be determinative on the level of nonlinearity and the global dynamics such that nonlinearity diminishes as the location of the polymer component gets closer to the middle of the structure; and the global dynamics changes from nonlinear hardening to softening as the thickness of the polymer coupling increases.

Acknowledgements

First, I would like to thank my research advisor, Dr. Hanna Cho. I started to know Dr. Cho when I was in her System Dynamics and Vibration class back in my junior year. Dr. Cho provided me with the opportunity to get involved in one of her research projects after we talked about my interests in research and my plan toward graduate school. With her understanding of my lack of experience in research, Dr. Cho asked her PhD student Keivan Asadi to train me with important technical skills. Dr. Cho is more like a life mentor instead of just a research advisor to me since I learned many things other than being a researcher from her, which include how to become a good cooperator and how to behave as a better person. Again, I want to thank Dr. Cho for her support on my research and my plan on graduate study.

Second, I would also like to thank all the members in Micro/Nano Multiphysical Dynamics Lab (MNMDL), especially to Keivan and Dr. Hatem Brahmi. Keivan trained me the FEA skills that I need for conducting simulations; he also helped me a lot on revising my thesis. Thank you so much for spending your time and effort and I will always memorize you not only as my research partner but also as my friend.

Third, I would like to show my appreciation to Professor Siston for being the mentor of the honor research class. I learned a lot from Professor Siston about doing presentation and writing thesis. It would be difficult for me to professionally present my research without his help.

Last but not least, I want to say thank you to my parents. There are some hard times that I have experienced during my undergraduate study; my parents always encourage me and provide me with confidence to face those challenges. Thank you!

Table of Contents

List of Figures

List of Tables

Chapter 1: Introduction

1.1 Motivation

Micro-electro-mechanical systems (MEMS) is a process technology that integrates mechanical and electronic components into compact systems, which are known for their excellent performance in sensing, controlling, and actuating [1]. MEMS technology is investigated for different fields including but not limited to hypersensitive sensors [3-6], radio frequency (RF) MEMS [7], Optical MEMS [8], signal processing elements [9], and logic devices [10-12]. Advanced microfabrication techniques make it possible for the batch fabrication of MEMS devices, which promotes the commercialization of MEMS. For example, MEMS sensor industry, one of the most-developed sectors of MEMS, produces many commercialized applications such as pressure sensors, accelerometers, gyroscopes, and temperature sensors that are being frequently used in our daily life.

MEMS devices usually consist of electronic components such as microprocessor for signal processing and mechanical components such as micro-sensors to interact with the surroundings. The performance of MEMS devices usually depends on the sensitivity of micro-resonator-based sensors, e.g. commercial MEMS oscillator [2], microring-resonator-based sensor [20], optical micro resonator chemical sensor [21], and electrostatic charge sensor [22]. Micro-resonators are commonly used as the main mechanical components in aforementioned micro-sensors and the functionality of these sensors largely relies on the dynamic behavior of micro-resonators. While linear micro-resonators are proved to be successful in sensing applications, more recent research attention is attracted by nonlinear micro-resonators since they have the potential to perform better than their linear counterparts. Such potential is reflected in their unique nonlinear features, e.g.

internal resonance [18], bifurcation [19, 23], hysteresis [23], and capability of avoiding limitations associated with applications of linear micro-resonators [24]. In addition, Nonlinearities are readily observed in dynamic responses of micro-resonators due to their small size and low damping, but well developed linear theories are not applicable to nonlinear systems as discussed by Younis in [15]. Thereby recent research efforts focus heavily on taking advantage of nonlinearities in their micro-resonator designs.

There are sources of nonlinearities in MEMS due to forcing [17], damping [14], and stiffness [13,14,15,16]; nonlinearity due to stiffness can be further divided into geometric [13, 14] and material nonlinearity [16]. In this research, we focus on geometric nonlinearity which can be controlled by tailoring the structural design of micromechanical resonators. While the nonlinear resonance has been investigated experimentally and analytically, this research focuses on investigating nonlinear characteristics within two micro resonator designs through finite element simulations to provide broad dynamic details that are useful for later analytical modeling and experiments.

1.2 Nonlinear Dynamics of Micromechanical Resonator

Figure 1 shows the frequency response curves of linear and nonlinear systems. In Fig. 1a, the linear frequency response is shown as a symmetric resonance curve with a narrow frequency bandwidth around the resonant frequency of a system. The frequency response curve bends toward higher frequencies when hardening stiffness nonlinearity is involved Fig. 1b; the nonlinear frequency response curve consists of two stable resonance branches (solid line) and an unstable resonance branch (dashed line). When the frequency is swept up from low frequencies, the resonant amplitude follows the upper stable resonance branch up to the largest amplitude point and then suddenly drops down to the lower stable branch; as the excitation frequency is swept

down from high frequencies, the resonant amplitude follows the lower stable branch up to a point where unstable branch occurs and then jumps upward to the upper stable branch. This phenomenon, known as hysteresis, means that for a given frequency within the range of the hysteresis loop, there are two corresponding resonant amplitudes. Such hysteresis loop does not exist in frequency responses of linear systems.

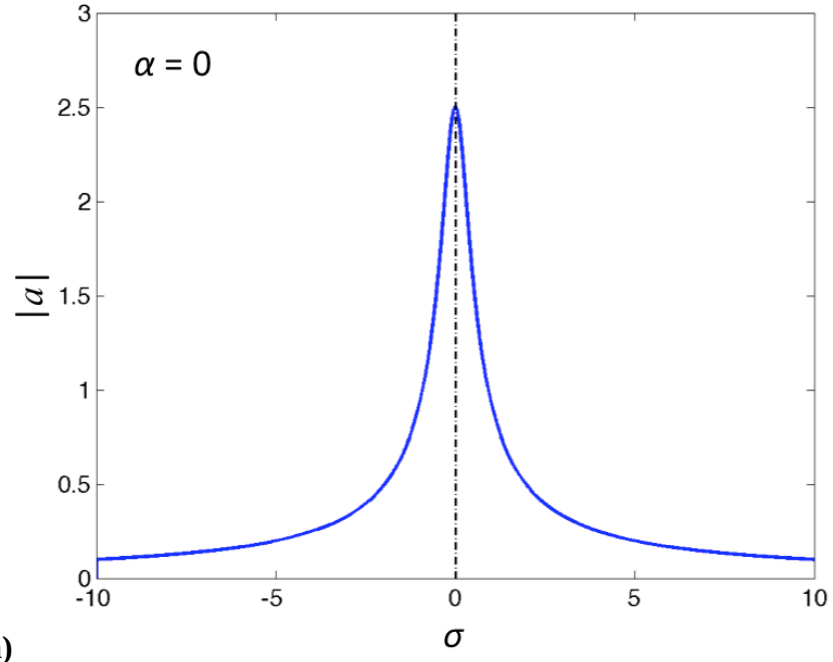

(a)

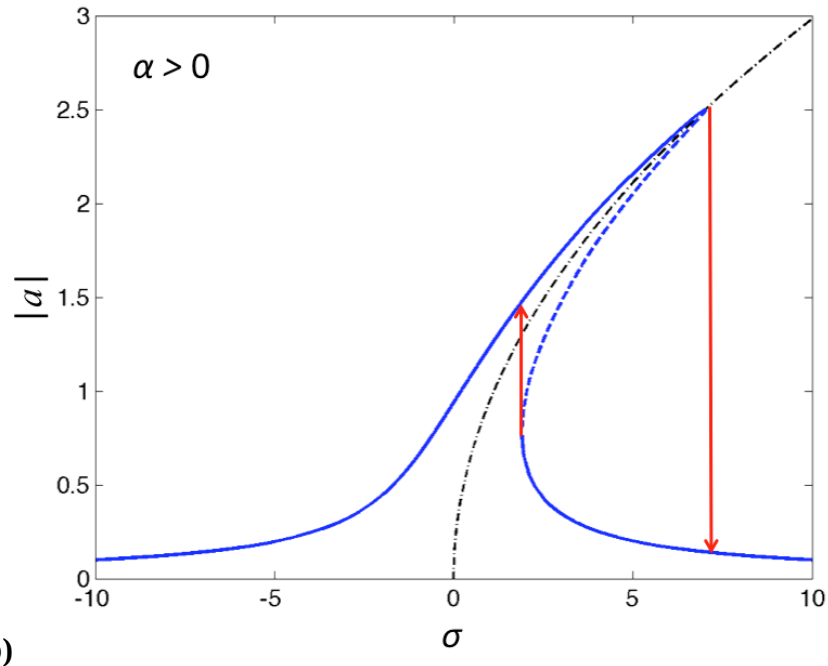

(b)

Figure 1: (a) linear frequency response curve; (b) nonlinear frequency response curve; α, a, and σ are the nonlinear constant, response amplitude, and frequency detuning parameter.

When a micro-beam resonator is oscillating with a large amplitude relative to its thickness, geometric nonlinearity is induced due to an increase of its stiffness caused by the midplane axial stretching within the structure. This axial tensile stress results in cubic stiffness nonlinearity. The axial the dynamics of a nonlinear system can be understood with a single degree of freedom (SDOF) spring-mass-damper system with a nonlinear spring as shown in Fig. 2. When a spring with linear and cubic nonlinear stiffness is employed in the system, the spring force is expressed by Eq. 1 and the equation of motion of this system is represented by Eq. 2.

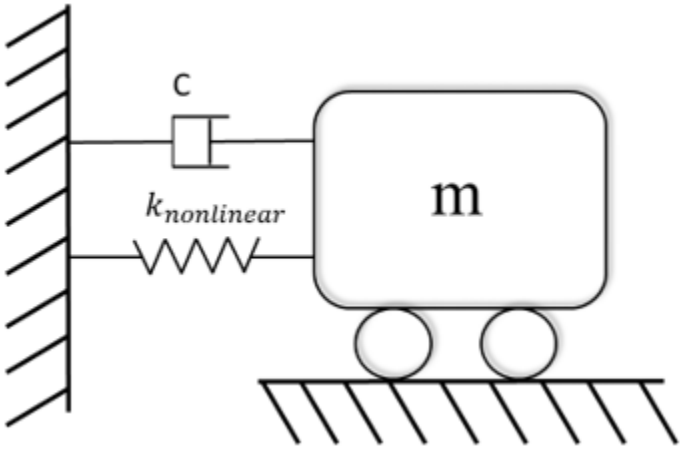

Figure 2: SDOF spring-mass-damper system with a nonlinear spring

$$F = k_1 x + k_3 x^3 \tag{1}$$

$$m\ddot{x} + c\dot{x} + k_1 x + k_3 x^3 = 0 \tag{2}$$

When the system is driven by a harmonic exciting force:

$$F(t) = F_o cos(\omega t) \tag{3}$$

where F_o is the amplitude of exciting force and ω is the excitation frequency, the equation of motion becomes:

$$m\ddot{x} + c\dot{x} + k_1 x + k_3 x^3 = F_o cos(\omega t) \tag{4}$$

Dividing Eq. 4 by *m* gives us:

$$\ddot{x} + 2\mu\dot{x} + \omega_o x + \alpha x^3 = q_o cos(\omega t) \tag{5}$$

where $\mu = \frac{c}{2m}$, $\omega_o = \frac{k_1}{m}$, $\alpha = \frac{k_3}{m}$, $q_o = \frac{F_o}{m}$, and ω are the damping, linearized resonant frequency, nonlinear constant, amplitude of exciting force, and excitation frequency.

The effect of the nonlinear constant α, excitation force q_0, and damping μ on the frequency response curves is shown in Fig. 3. Figure 3a illustrates that the bending direction and extent of the frequency response curve are determined by the nonlinear constant α. *As* α decreases from a positive value to a negative one, the response switches from nonlinear hardening to softening. To make it clear, nonlinear hardening resonance is identified when the response curve bends toward higher frequencies

and softening resonance means that the response curve bends toward lower frequencies. Figure 3b shows the transition of a system from linear to nonlinear hardening resonance as excitation force q_0 increases. In Fig. 3c, the response curve becomes sharper and the peak amplitude increases as the damping μ decreases; when we take the damping μ to be zero, the resonant peak amplitude becomes infinite and the response curve approaches to the black dashed line, which is known as the backbone curve. In fact, all the frequency-amplitude dependences are shown as black dashed lines in Fig. 3 and are called backbone curves, which correspond to the responses of nonlinear free vibrations without damping.

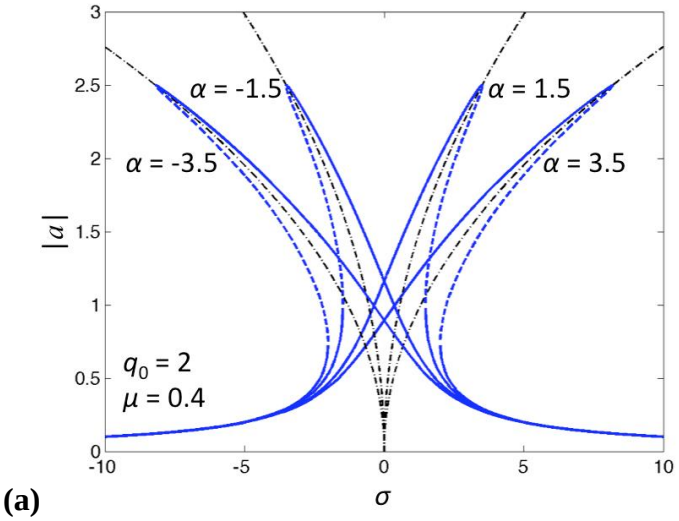

(a)

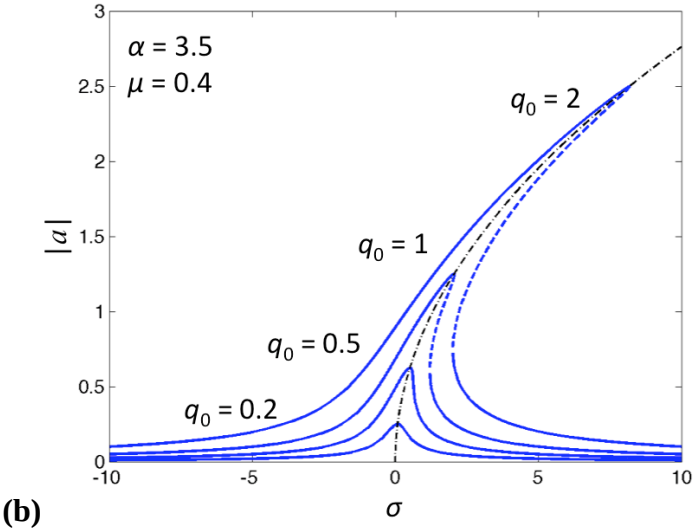

(b)

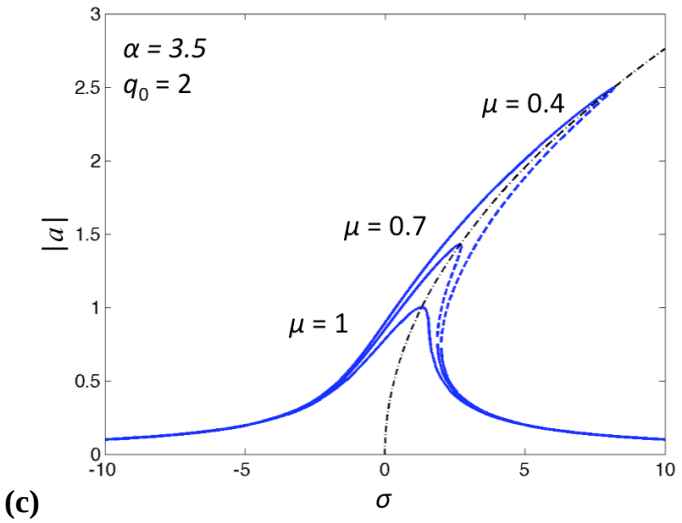

Figure 3: Frequency response curves under the influence of (a) nonlinear constant α, (b) excitation force q_0, and (c) damping μ.

1.3 Finite Element Analysis

Finite element analysis (FEA) is the application of finite element method (FEM), which typically starts with dividing the domain of the problem into many subdomains known as "finite elements". Here, "finite" refers to the limited number of degrees of freedom being used to simulate the behavior of the object. Dividing a domain into simpler subdomains has many advantages [25] such as accurate modeling of complex geometries, detailed capture of local effects, and inclusion of different material properties. Therefore, FEA is always utilized as a computational tool for conducting engineering analysis.

In this work, FEA is used to analyze silicon micro-cantilever-polymer systems exhibiting strong nonlinear behaviors. Younis [15] suggests that while perturbation and asymptotic approaches are used for analyzing weak nonlinearities, numerical approaches, e.g. FEA, are needed for analyzing strong nonlinearities. FEA is conducive to designing nonlinear micro-resonators because it can provide various field outputs at any location of the micro-resonators during nonlinear resonance. While field outputs including displacement, velocity, and acceleration can be obtained both experimentally and numerically, other important outputs such as strain, stress,

and force are attainable with FE simulations only. In addition, FEA can accurately estimate the level of nonlinearity even before fabricating the devices and design criteria can be obtained based on simulation results.

The proposed FEA methodology is based on imposing a deflection to the structure at the corresponding mode shape and releasing it from a relatively large amplitude to have the structure experience the free decay response. The FEA methodology is validated by experimental results and it is considered as a new strategy for justifying analytical assumptions of nonlinear micro-resonator designs. FE simulations are conducted for two types of structures including single and double silicon micro-cantilevers with a polymer coupling. To investigate the global dynamics of these structures, backbone curves and frequency content graphs, e.g. fast Fourier and wavelet transforms, are obtained during postprocessing. The effect of geometrical dimensions and material properties of the polymer component on the level of nonlinearity has been studied with FEA and design criteria for achieving desired nonlinear behaviors are obtained.

1.4 Objectives

This research seeks to take advantage of FEA as a complementary approach to experimental characterization and analytical modeling in designing tunable nonlinear micro-systems. The main objectives of this research are listed below:

1. Characterize the global dynamics for two types of nonlinear micro-resonator designs through FE simulations.
2. Obtain design criteria to calculate the targeted level of nonlinearity for both types of structures.
3. Utilize FEA as a numerical approach to verify analytical assumptions.

Chapter 2: Methodology

2. 1 Preprocessing: Description of FEA Models

2.1.1 Single Silicon Micro-Cantilever-Polymer Structure

The first nonlinear micromechanical system studied in this work is composed of a single silicon micro-cantilever bridged to the ground by a polymer coupling as shown in Fig. 4. In this design, stiffness nonlinearity is intentionally introduced into an otherwise micro-cantilever system by integrating a polymer coupling. The dynamics of the Si micro-cantilever itself is linear because its free end can release the axial tension even at large oscillation amplitude. The polymer coupling will introduce axial tension when the Si cantilever oscillate at a large oscillation in the vertical (out-of-plane) direction.

A large effective stiffness difference between the silicon cantilever and the polymer coupling is intentionally tailored. Based on the geometrical dimensions and material properties of the structure, we can calculate the bending stiffness and axial stiffness for the two parts using the following equations:

$$k_{bending} = \frac{3EI}{L^3} \tag{6}$$

$$k_{axial} = \frac{EA}{L} \tag{7}$$

According to Eq. 6 and Eq. 7, the ratio of bending stiffness between the silicon cantilever and polymer coupler is calculated to be 0.15:1 and the ratio of axial stiffness between these two parts is 33.33:1. Therefore, a larger bending deflection in the silicon component is introduced by the bending force due to its relatively lower bending stiffness, while the polymer component experiences axial stretching easily due to its relatively lower axial stiffness. In this design, the only source of nonlinearity is the stiffness nonlinearities induced by the stretching within the polymer

component, which is caused by the large bending displacement of the free end of the silicon cantilever when the system is oscillating at one of its mode frequencies.

Figure 4: SEM image of single silicon micro-cantilever-polymer structure (dimensions: 500μm × 100μm × 2μm) with a polymer coupling (dimensions: 50μm × 12μm × 3μm) [14]

A 3D model shown in Fig. 5 is built using ABAQUS 6.14 (Hibbit Inc., Providence, Rhode Island) for this structure with the boundary conditions defined as clamped-clamped. The length, width, and thickness of the silicon cantilever are 500μm, 100μm, and 2μm; the length, width, and thickness of the polymer coupling are 50μm, 12μm, and 3μm. The young's modulus, density, and Poisson's ratio of silicon are 180GPa, 2330kg/m^3, and 0.28; and those of the polymer component are 3GPa, 1400kg/m^3, and 0.34.

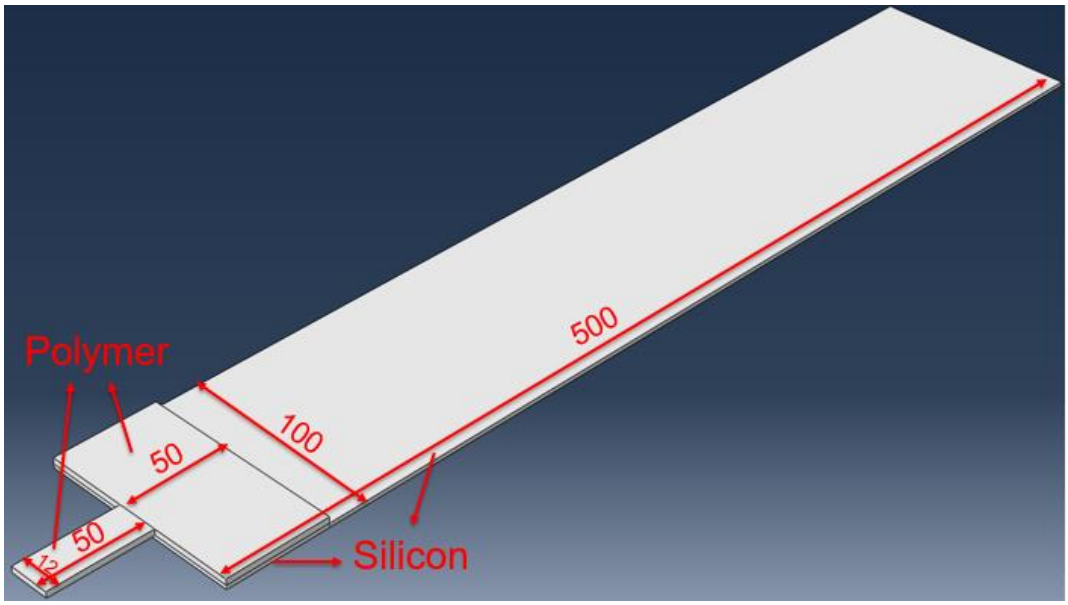

Figure 5: 3D model of the single cantilever-polymer structure

The model shown in Fig. 6 is finely meshed with sufficient number of linear reduced order hexagonal elements for accurate modal and implicit dynamic analyses. This model is partitioned into three sections including the polymer attachment section, polymer-silicon overlap section, and silicon cantilever section. The polymer attachment section is meshed into 800 (25×8×4) elements; the polymer-silicon overlap section is meshed into 960 (24×10×4) elements; the silicon cantilever section is meshed into 4320 (45×24×4) elements. Each section is assigned with at least 4 nodes on the thickness to ensure the accuracy of the simulation. Convergence study is conducted to ensure the mesh quality; linear element is selected for the element type instead of quadratic element to save the time of simulation process.

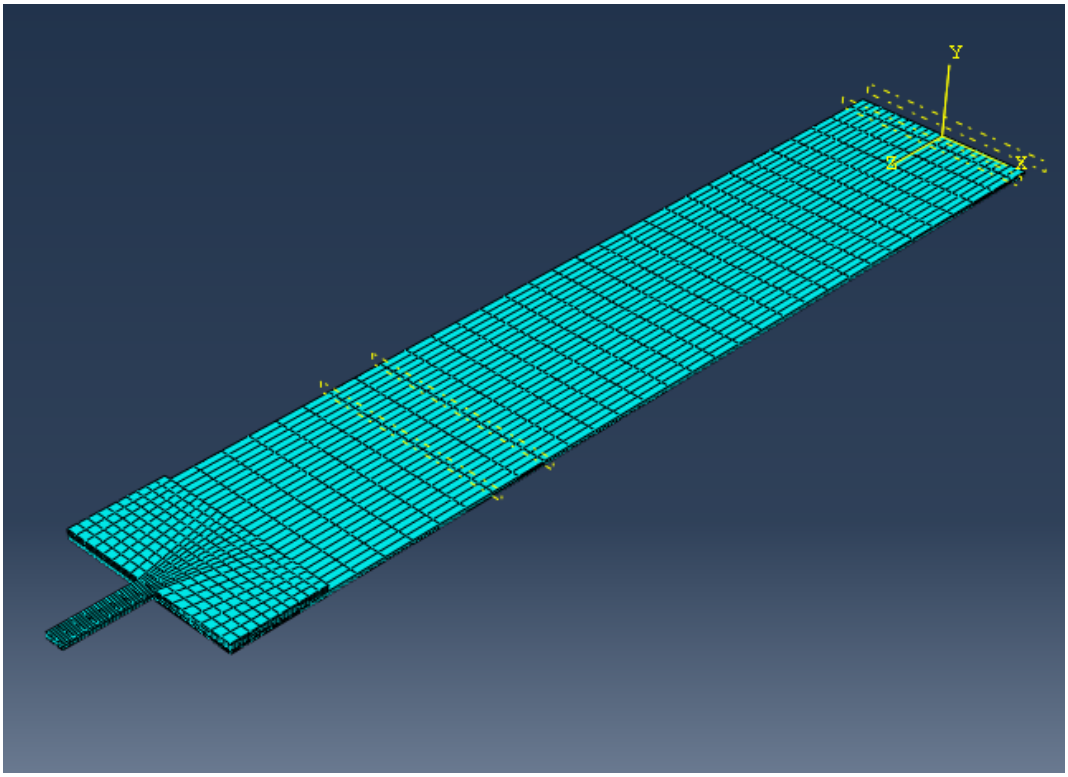

Figure 6: Meshing the single cantilever-polymer structure model with linear reduced order hexagonal elements

2.1.2 Double Silicon Micro-Cantilever Structure

An optical microscope image of the representative double cantilever-polymer structure considered in this work is depicted in Fig. 7. This system consists of two silicon micro-cantilevers bridged by a polymer coupling between two free ends and the structure is fixed to the ground on the other ends. As in the aforementioned single-cantilever-polymer system, the polymer coupling is integrated to induce axial tension and, thereby, geometric nonlinearity in the whole system, when two cantilevers are oscillating in the vertical direction.

The width and thickness of the silicon cantilevers are 40μm, and 2μm; and the length of each cantilever varies from 25μm to 250μm while the total length of the two is maintained at constant value, 500μm. The length, width, and thickness of the polymer coupling are 20μm, 7μm, and, 1.5μm. The young's modulus, density, and Poisson's ratio of silicon are 180GPa, 2330kg/m^3, and 0.28; and corresponding material properties of polymer are 3GPa, 1400kg/m^3, and 0.34.

Similar to the single cantilever-polymer system, stiffness nonlinearity is induced into these otherwise linearly-behaved cantilevers through implementing the polymer coupling when it is stretched during oscillation of the system.

In this thesis, six configurations of double cantilever-polymer structure are included and depicted as "A_B" such that "A" represents the length of the shorter cantilever and "B" defines the length of the longer cantilever with units in micrometers. These configurations are "25_475", "50_450", "100_400", "175_325", "225_275", and "250_250". The representative double cantilever-polymer structure shown in Fig. 7 is configuration "50_450".

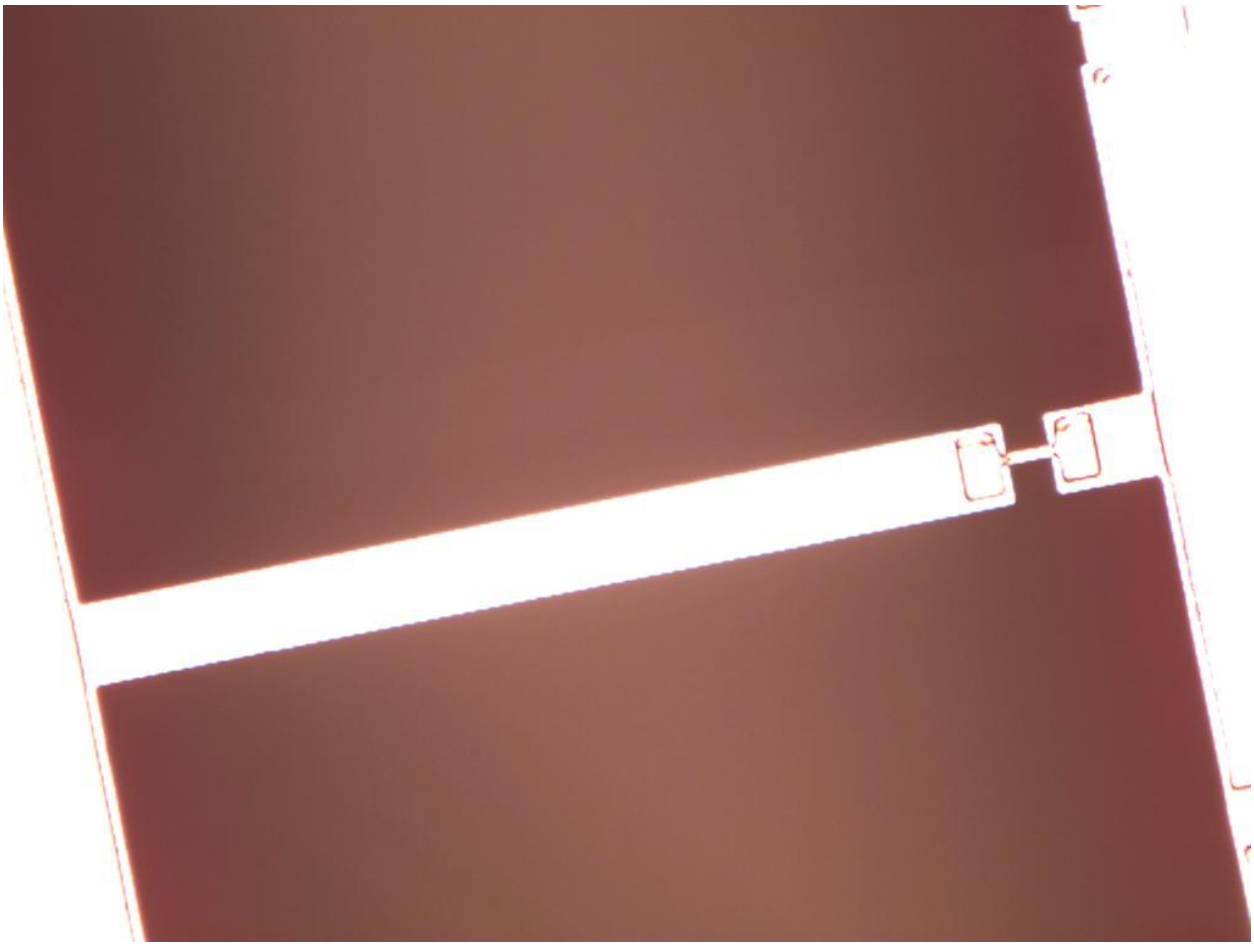

Figure 7: Optical microscope image of double silicon cantilever-polymer structure (Length of the left cantilever = 450μm; length of the right cantilever = 50μm)

To accurately simulate the global dynamics of double cantilever structures, several 3D models, e.g. Fig. 8, were built for these systems with boundary condition taken as clamped-clamped. The width and thickness of the silicon cantilevers are 40μm, and 2μm; and the length of each cantilever varies from 25μm to 250μm while the total length of the two is maintained at constant value, 500μm. The length, width, and thickness of the polymer coupling are 20μm, 7μm, and, 1.5μm. The young's modulus, density, and Poisson's ratio of silicon are 180GPa, 2330kg/m^3, and 0.28; and corresponding material properties of polymer are 3GPa, 1400kg/m^3, and 0.34.

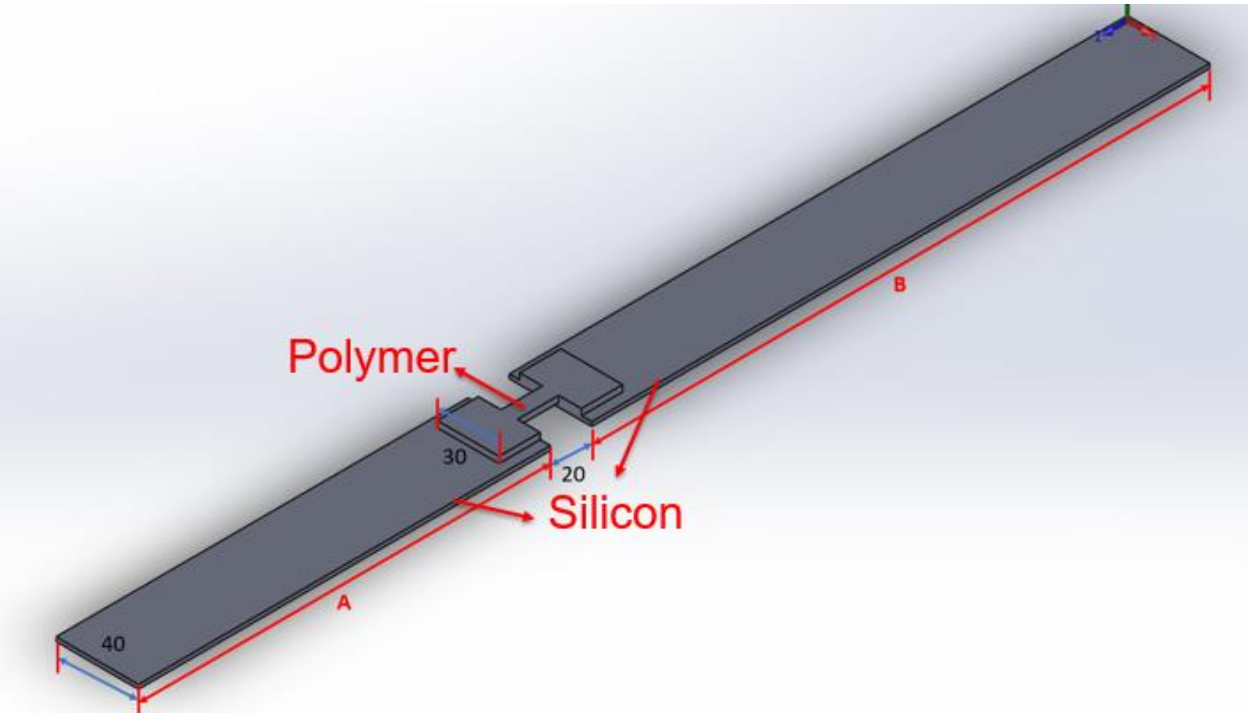

Figure 8: 3D model of the double cantilever-polymer structure

These models were finely meshed with sufficient number of linear reduced order hexagonal elements for accurate modal and implicit dynamic analyses. Figure 9 shows an example of properly meshed double cantilever structure. The double cantilever models are divided into three sections including polymer coupling section, two polymer-silicon overlap sections, and silicon micro-cantilever section. The polymer coupling section is meshed into 160 (10×4×4) elements; the polymer layer of a polymer-silicon overlap section is meshed into 192 (12×4×4) elements, while

the silicon layer of an overlap section is meshed into 256 (16×4×4) elements; the silicon micro-cantilever section is meshed into 2944 (46×16×4) elements. Based on convergence study, each section is assigned with at least 4 nodes on the thickness to ensure the mesh quality. Linear element is selected for the element type instead of quadratic element to save the time of simulation process.

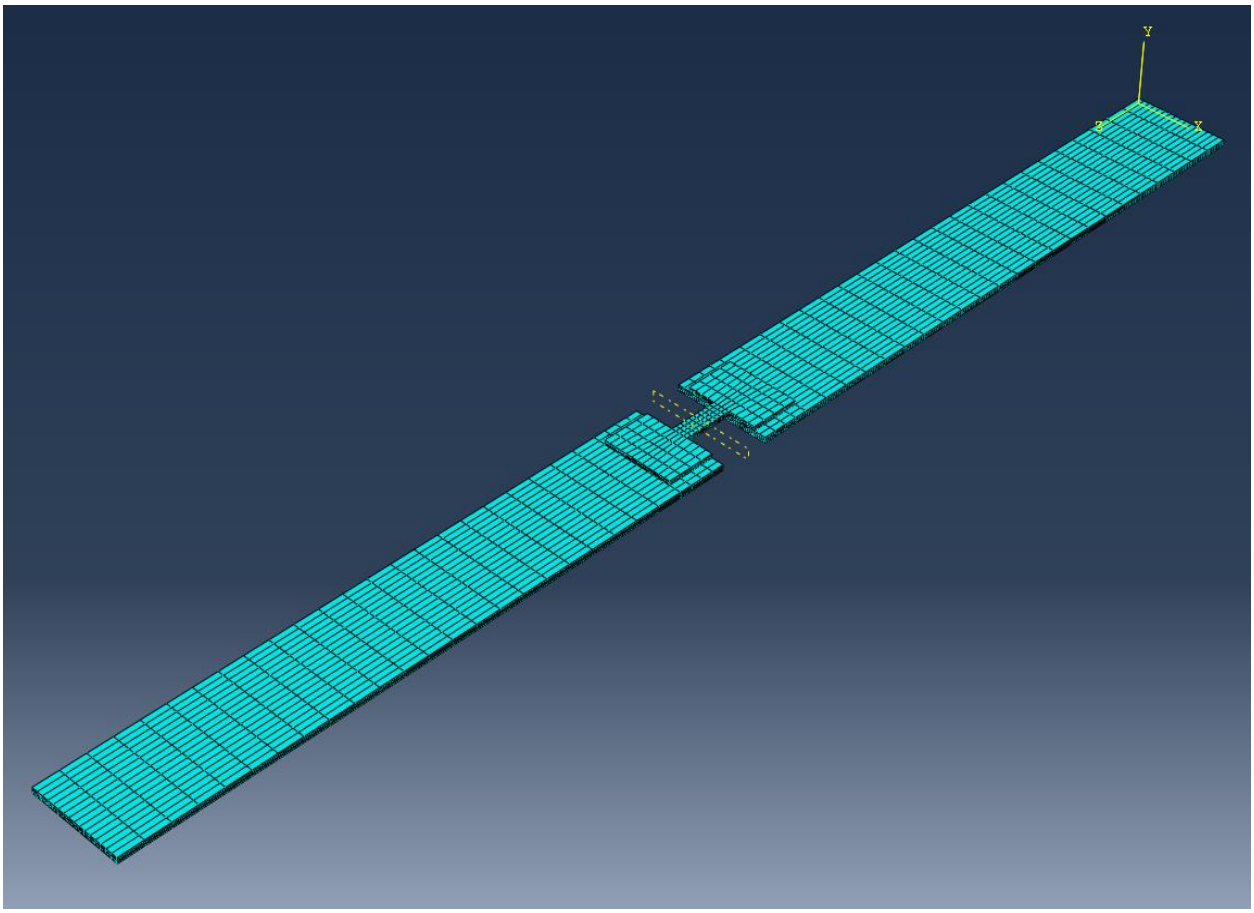

Figure 9: Meshing the double cantilever-polymer structure model with linear reduced order hexagonal elements; configuration (250_250)

2.2.3 Modal Analysis Simulation

Modal analysis simulation is conducted to determine the linear mode frequencies and mode shapes of the micro-resonators. The eigenvalue of this analysis step is set to be 5 since this research mainly focuses on the first few modes, which dominate over higher modes within a vibrating system. To validate proposed FEA methodology, simulated mode frequencies are compared with experimentally obtained resonant frequencies.

Simulated mode shapes are extracted to generate the associated mathematical functions that will be imposed to the model for implicit dynamic analysis. The process of generating mode shape function is illustrated in Fig. 10. To obtain the mode shape of interest, a path in Fig. 10a is assigned along the *z* direction so that the "*z*-*y*" data representing the mode shape can be collected as shown in Fig. 10b. The collected mode shape data are then fitted with Sum of Sines Model using MATLAB's build-in application "Curve Fitting". Figure 10c and 10d are the fitted curve and mode shape function, respectively. This mode shape function, i.e. sum of sines, is then imposed on the structure as an analytical field, which serves as the initial condition of the dynamic simulation.

Note that for modes higher than the first mode, we only fit the curve for the silicon cantilever part because there is an abrupt slope change at where the polymer coupling and the silicon cantilever is connected; the large difference between the slopes of the two parts makes it different to properly fit the curve for the entire structure.

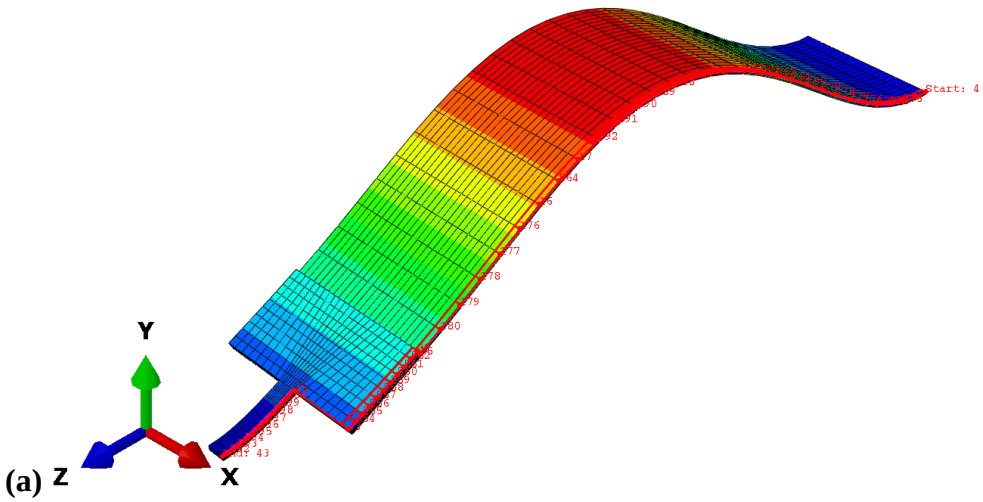

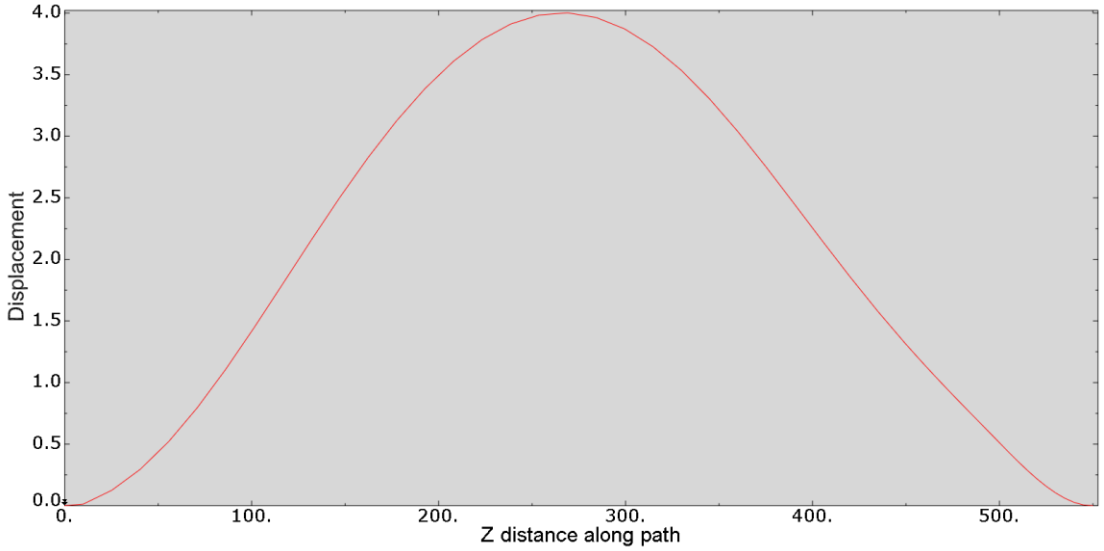
Displacement
4.0
3.5
3.0
2.5
2.0
1.5
1.0
0.5
0.0
0.
100.
200.
300.
400.
500.
Z distance along path

(b)

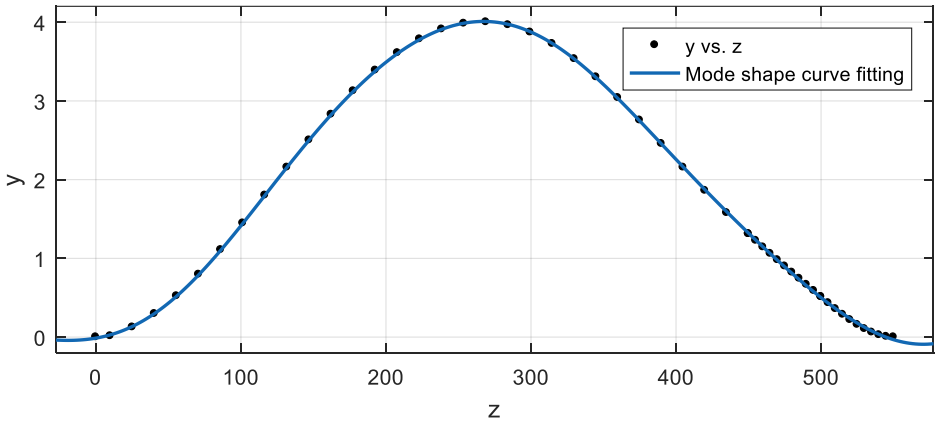
y vs. z
Mode shape curve fitting
y
z
0
1
2
3
4
0
100
200
300
400
500

(c)

General model Sin4:
f(x) =
a1*sin(b1*x+c1) + a2*sin(b2*x+c2) + a3*sin(b3*x+c3) +
a4*sin(b4*x+c4)
Coefficients (with 95% confidence bounds):
a1 = 2.562 (-1.901, 7.025)
b1 = 0.003557 (-0.009096, 0.01621)
c1 = 0.5799 (-2.784, 3.944)
a2 = 0.8234 (-1963, 1964)
b2 = 0.02958 (-0.6102, 0.6693)
c2 = 1.632 (-155.8, 159.1)
a3 = 1.444 (-2.881, 5.77)
b3 = 0.01206 (2.414e-05, 0.02409)
c3 = -1.646 (-4.625, 1.334)
a4 = 0.8007 (-1963, 1964)
b4 = 0.0301 (-0.5938, 0.6541)
c4 = 4.644 (-151.8, 161.1)

Goodness of fit:
SSE: 0.005654
R-square: 0.9999
Adjusted R-square: 0.9999
RMSE: 0.01174

(d)

Figure 10: Process of generating mode shape function: (a) single cantilever-polymer structure at its first mode with a path assigned on its front edge; (b) collected "z-y' data of the path; (c) fitted curve based on the collected data; (d) mode shape function of the fitted curve.

2. 2 Postprocessing

2.2.1 Backbone Curve

In implicit dynamic analysis, the structure is released from a relatively large initial deflection to have the structure experience the free decay response as shown in Fig. 11a. To better understand the nonlinear behavior of micro-beam resonators, backbone curve is introduced as a tool to visualize the level of nonlinearity. Backbone curve defines the resonant frequency of a system as a function of its oscillation amplitude while taking the values of damping and forcing as zeros; nonlinearity is presented when the backbone curve bends toward either higher or lower frequencies. The process of generating backbone curves can be understood with a representative example shown in Fig. 11. In Fig. 11a, the simulated free decay response is obtained at the point of maximum deflection of the single cantilever-polymer structure when it is released at its first

flexural mode. The simulated backbone curve (red line) is generated from the simulated free decay response by calculated the resonant frequencies (i.e., the inverse of the periods) as a function of the oscillation amplitude with a developed MATLAB code shown in Fig. 24. The experimental data that collects resonant peak amplitudes under different driving amplitudes are shown as the blue dots in Fig. 11b, which are fitted into an experimentally obtained backbone curve (blue line). A comparison can be made between simulation and experimental results when normalized curves are plotted in one figure.

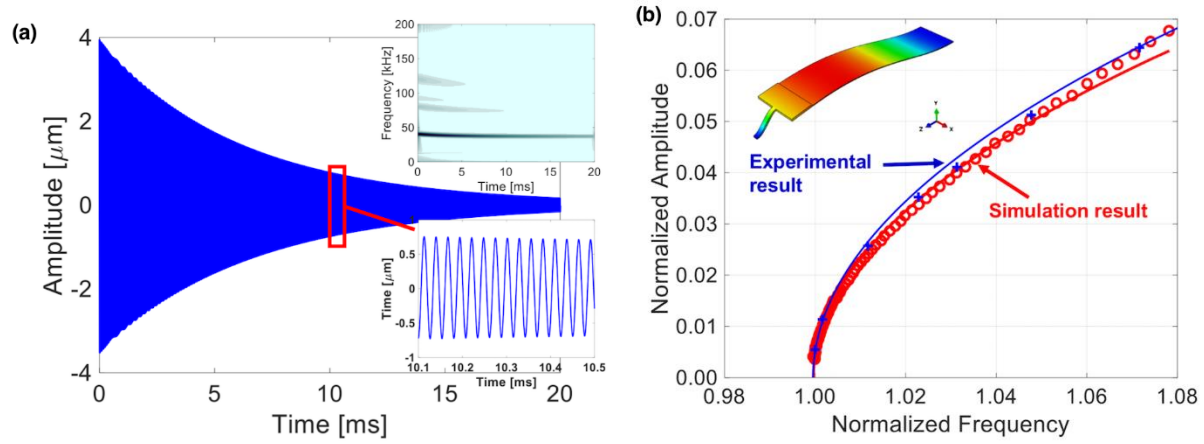

Figure 11: (a) The free decay response of the single cantilever-polymer structure when it is released at its first mode. The upper inset is the corresponding wavelet transform plot showing that the dominant mode is its first mode. The lower inset is an enlarged figure of a portion of the oscillating motion; (b) Simulated (red line) and experimentally obtained (blue line) backbone curves. [14]

2.2.2 Frequency Content Graphs

Frequency content graphs, e.g., fast Fourier transform (FFT) and wavelet transform (WT) plots, are obtained following postprocessing the dynamic response. FFT computes a series of discrete Fourier transform so that a signal in the time domain can be converted into the frequency domain; the FFT algorithm is shown in Fig. 22. WT plots are created to visualize the variations of signal frequencies with respect to time; Figure 23 shows the MATLAB code for generating WT plots. FFT identifies engaged frequencies in a signal without a time localization while WT describes what frequencies are presented and their participation throughout the simulation

response. Therefore, FFT is used to identify engaged frequencies of a response so that a signal filter, e.g. Fig. 23, can be developed to prevent the backbone curve from distortion; WT is useful when a system shows different dynamics at different oscillation amplitudes, e.g. internal resonance.

Figure 12 shows an example of frequency content graphs; FFT and WT plots are obtained from the free decay response of the (250_250) double cantilever structure when releasing it from a relatively large amplitude with its first mode being taken as the initial condition; the plots indicate that the first mode is dominantly excited in the structure which conforms to the initial condition assigned to the structure during preprocessing.

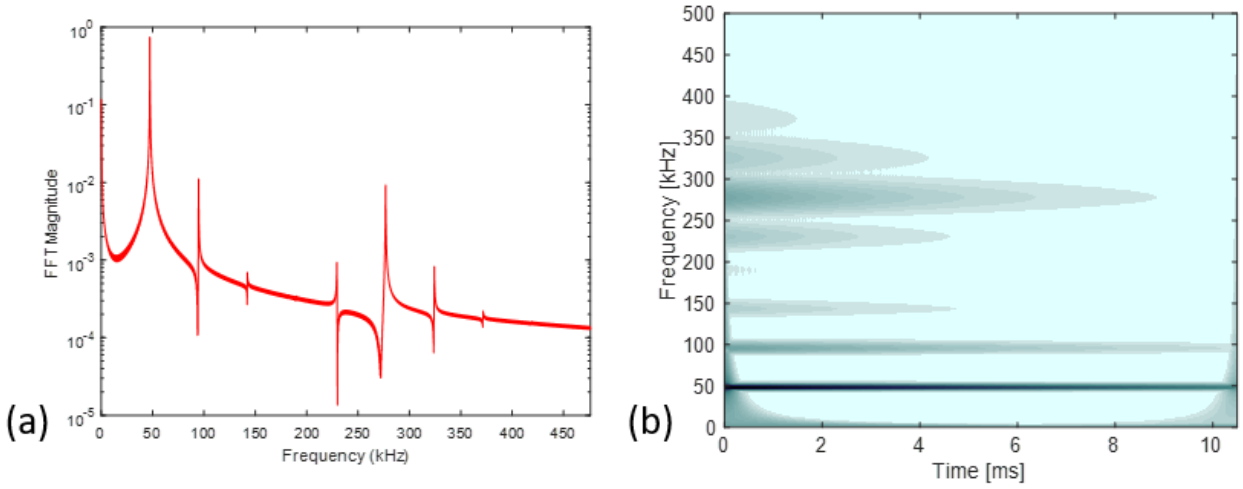

Figure 12: Fast Fourier Transform (a) and Wavelet Transform (b) of the double cantilever-polymer structure with configuration of (250_250)

Chapter 3: Results and Discussion

3.1 Single Silicon Micro-Cantilever Structure

3.1.1 Modal Analysis Results

Linear modal analysis was conducted for FEA models to obtain linearized mode frequencies and mode shapes. Figure 13 shows the first three flexural mode shapes of the single cantilever-polymer structure. Simulated mode frequencies of the first three flexural modes are all

very close to the experimentally obtained resonant frequencies; and the relative differences among these numerically and experimentally obtained frequencies are within 3.6% as shown in Table 1. Therefore, the proposed FEA methodology is proved to be accurate and we can proceeded to dynamic analysis.

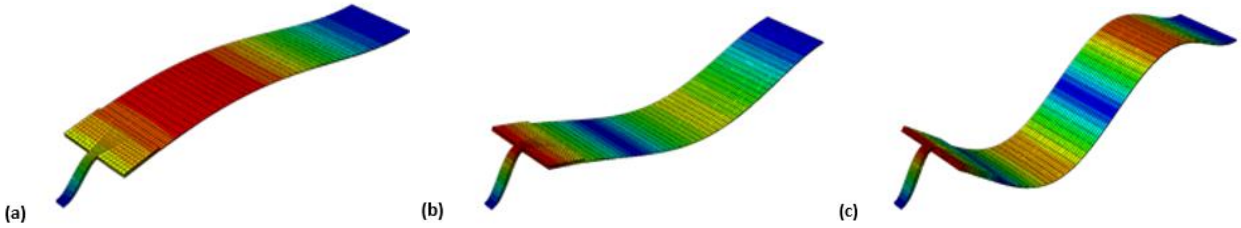

Figure 13: The first three flexural mode shapes of the single cantilever-polymer structure

Table 1: Comparison between numerically and experimentally obtained modal frequencies in a single cantilever structure.

		Flexural Modes		
		1	2	3
Resonant Frequency	Experiment (kHz)	37.6	89.5	203.4
	Simulation (kHz)	36.5	86.4	199.1
	Relative Difference (%)	3.01	3.59	2.16

3.1.2 Backbone Curve

Simulated backbone curves shown in Fig. 14 are generated when the structure is released at its first three flexural modes; they are compared with backbone curves obtained based on

experimental results. The simulated and experimentally obtained backbone curves show a good agreement in these plots.

Figure 24 shows a developed MATLAB code for calculating nonlinear coefficients. Simulated nonlinear coefficients are compared with those obtained from experimental data as shown in Table 2. The relative differences between simulated and experimentally obtained nonlinear coefficients for the first, second, and third mode are 11.72%, 29.07%, and 4.14%. Such a high level of accordance agrees with our observation on backbone curves; the result also indicates that strong nonlinearity exhibit not only in the first but also in higher flexural modes when a nonlinear component is introduced into an otherwise linear component.

Table 2: Comparison between numerically and experimentally obtained nonlinear coefficients for single cantilever structure.

		Flexural Modes		
		1	2	3
Nonlinear Coefficient (α)	Experiment	414.8	1041.4	473.4
	Simulation	463.4	806.8	493.0
	Relative Difference (%)	11.72	29.07	4.14

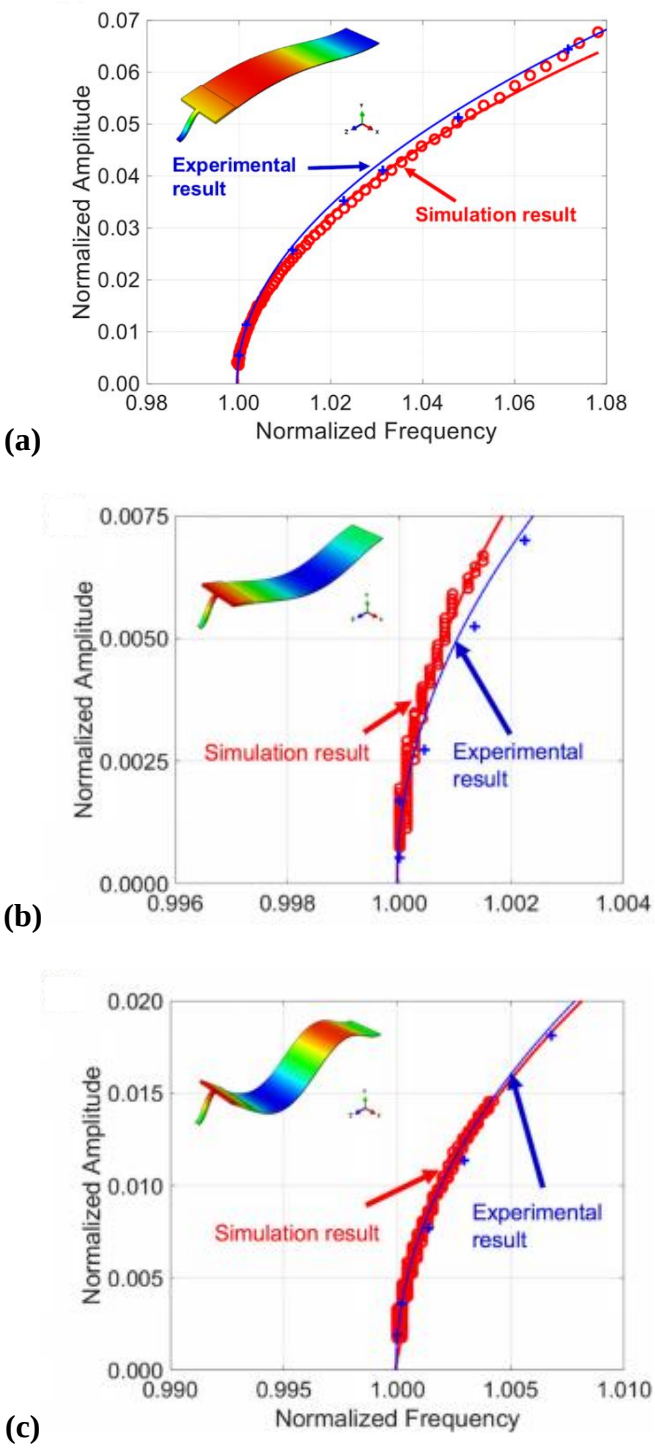

Figure 14: Experimentally obtained (blue line) and simulated (red line) backbone curves at the single cantilever-polymer structure's (a) first mode, (b) second mode, and (c) third mode. [14]

3.1.3 Design Criteria

In this research, a design criterion, i.e. stiffness of the nonlinear component, for single cantilever structure is obtained when FEA is utilized as the numerical approach. Figure 15 shows the simulated backbone curves when different values of Young's modulus of polymer component are employed; the global dynamics switches from nonlinear hardening to softening as the polymer component gets stiffer. Although it is impractical to alter Young's modulus automatically, we can use materials with different stiffness for the nonlinear component to achieve desired nonlinear behavior. Therefore, different nonlinear behaviors in single cantilever structures are attainable by tuning the stiffness of the nonlinear component. Note that we assume the density of the nonlinear component to be consistent while simulating the dynamic behaviors of the system with different stiffness. Although the density can vary with different values of Young's modulus, we ignore this variation because the size and mass of nonlinear component are remarkably smaller than those of the cantilever part.

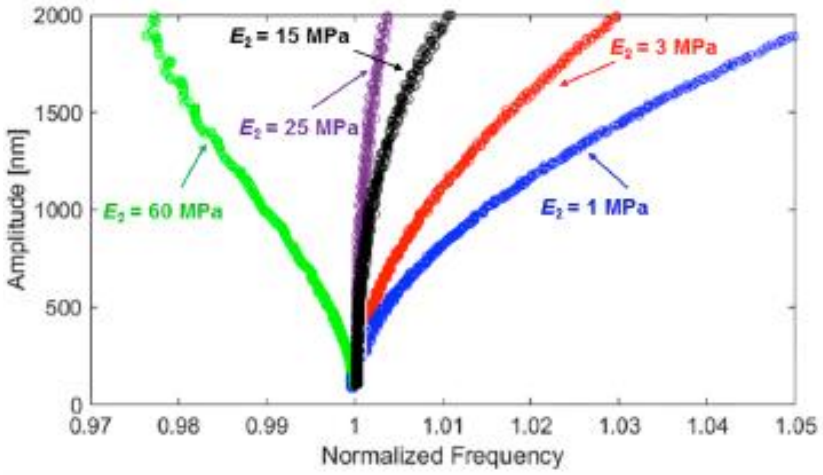

Figure 15: An increase in the Young's modulus of the nonlinear component of the structure switches the global dynamics from nonlinear hardening to softening. [14]

3.1.3 Verification of Analytical Assumptions

The proposed analytical model is shown in Fig. 16; the vertical mass-spring-damper system represents the silicon cantilever while the polymer component is represented by the horizontal mass-spring-damper system. This model is assumed to be moving only in the vertical direction representing the oscillation motion of the system. In this case, the polymer component is always being stretched when the silicon cantilever is only oscillating back and forth in the vertical direction; the axial stretching in the polymer component serves as the origin of geometric nonlinearity as discussed earlier.

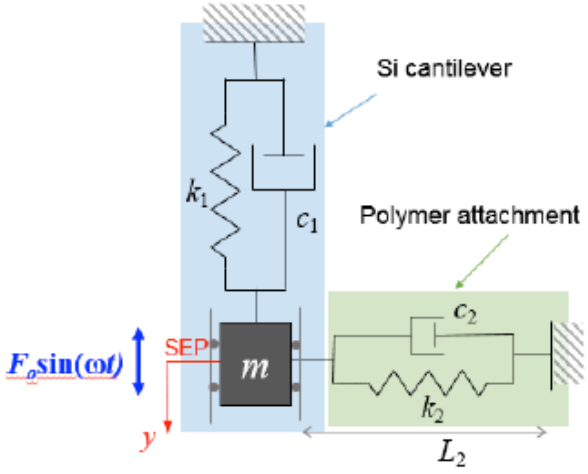

Figure 16: Proposed lumped parameter model of the single cantilever-polymer structure. [14]

To verify the assumptions made for analytical model about the origins of nonlinearity, the axial strain responses are investigated for both silicon and polymer components. The axial strain response (blue line) of the polymer component is obtained together with its averaged value (red line) at its midplane as shown in Fig. 17a. Averaged axial strain is always positive and increases with increasing oscillation amplitude. The inset of Fig. 17a indicates that the oscillating frequency of the polymer strain response (red line) is twice as fast as that of the displacement response (blue line). For the silicon component, the axial strain response (blue line) is also obtained together with its averaged value (red line) at midplane of the cantilever as shown in Fig. 17b. Averaged axial

strain remains at zero throughout the simulation. The inset shows that the oscillating frequency of the silicon strain response (red line) is the same as that of the displacement response (blue line). Investigations on the axial strain responses indicate that the stretching within the polymer component serves as the nonlinear origin and the silicon component behaves linearly. Therefore, the proposed analytical assumptions are verified.

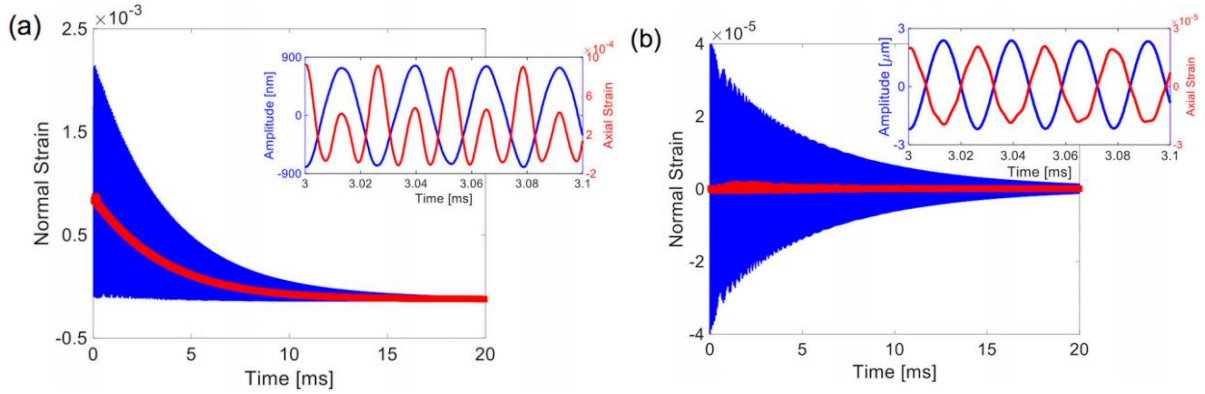

Figure 17: (a) The axial strain response obtained at the midplane of the polymer component (blue) with the averaged value of the response (red). The inset figure compares the axial strain response (red) with the displacement response (blue); (b) The axial strain response obtained at the midplane of the silicon component (blue) with the average value of the response (red). The inset figure compares the axial strain response (red) with the displacement response (blue). [14]

3.2 Double Silicon Micro-Cantilever Structure

3.2.1 Modal Analysis Results

Figure 18 shows the first flexural mode shapes of all six configurations of double cantilever structure. Simulated mode frequencies of the first two flexural modes are obtained from modal analysis; the largest relative differences among these numerically and experimentally obtained frequencies is 31.77% as shown in Table 3. The relative differences are generally larger comparing to that of the single cantilever structure for two reasons. First, the material properties, which are determinative to modal analysis, vary from case to case for the actual samples used in experiments, thereby larger relative difference occurs when consistent material properties are used for

simulations. Second, an increase in the complexity of the structure might decrease the accuracy of the analysis.

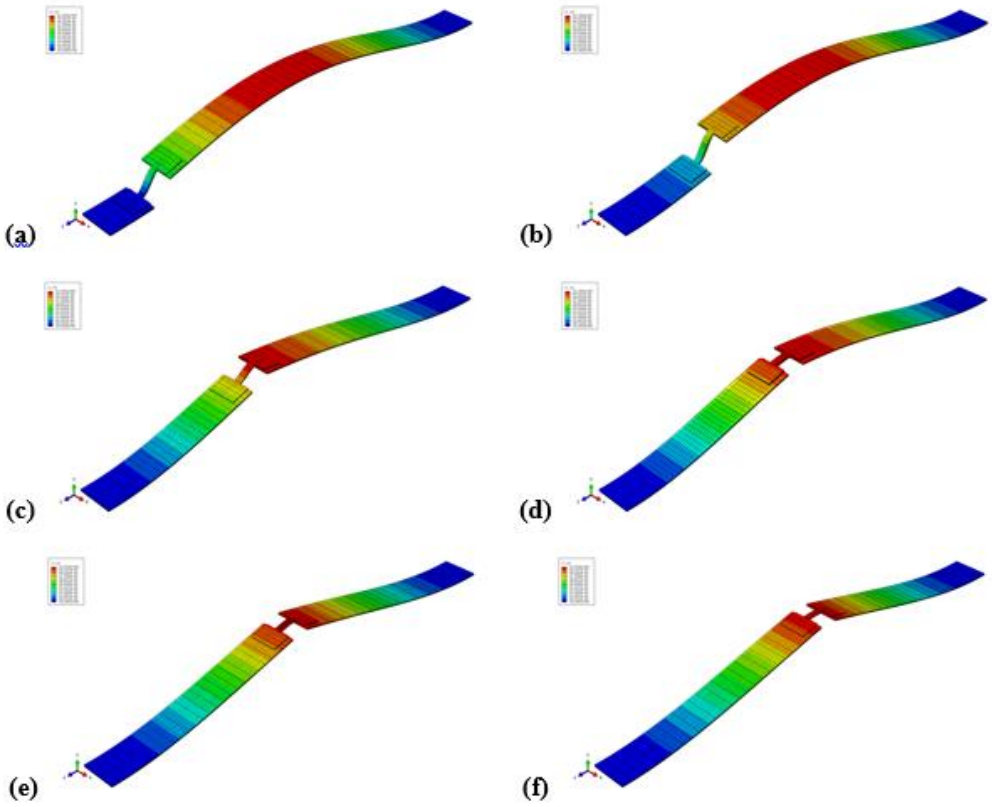

Figure 18: First mode shape of double cantilever structures with configurations (length A_ length B) of (a) 25_475; (b) 50_450; (c) 100_400; (d) 175_325; (e) 225_275; (f) 250_250

Table 3: Comparison between numerically and experimentally obtained mode frequencies for different configurations of double cantilever structures.

Configurations (length1_length2)	Simulation (kHz)		Experiment (kHz)		Relative Difference (%)	
	Mode 1	Mode 2	Mode 1	Mode 2		
25_475	52.9	134.7	67.0	170.0	21.11	20.76
50_450	52.2	131.0	71.0	177.0	26.50	26.00
100_400	57.6	138.3	77.0	173.0	25.64	20.03

175_325	58.8	154.1	75.0	170.0	21.63	9.34
225_275	53.4	156.2	70.0	185.0	23.74	15.59
250_250	47.4	139.9	69.5	184.0	31.77	23.96

3.2.2 Backbone Curve

In Fig. 19, backbone curves of the six configurations are obtained when the structure is released at its first flexural mode. Simulated nonlinear coefficients, which are calculated using the MATLAB code shown in Fig. 25, are characterized for all six configurations. The simulated nonlinear coefficients of configurations (250_250), (225_275), (175_325), (100_400), (50_450), and (25_475) are -2.92e-08, -1.67e-8, 2.46e-8, 2.13e-8, 2.22e-7, and 2.36e-7. This agrees with the trend as shown in Fig. 19b such that the level of nonlinearity diminishes as the polymer component moves from the end to the middle of the structure.

Table 4: Simulated nonlinear coefficients for different configurations of double cantilever structures when structures are released at the first mode

Configurations (lengthA_lengthB)	250_250	225_275	175_325	100_400	50_450	25_475
Simulated Nonlinear Coefficient	-2.92e-08	-1.67e-8	2.46e-8	2.13e-7	2.22e-7	2.36e-7

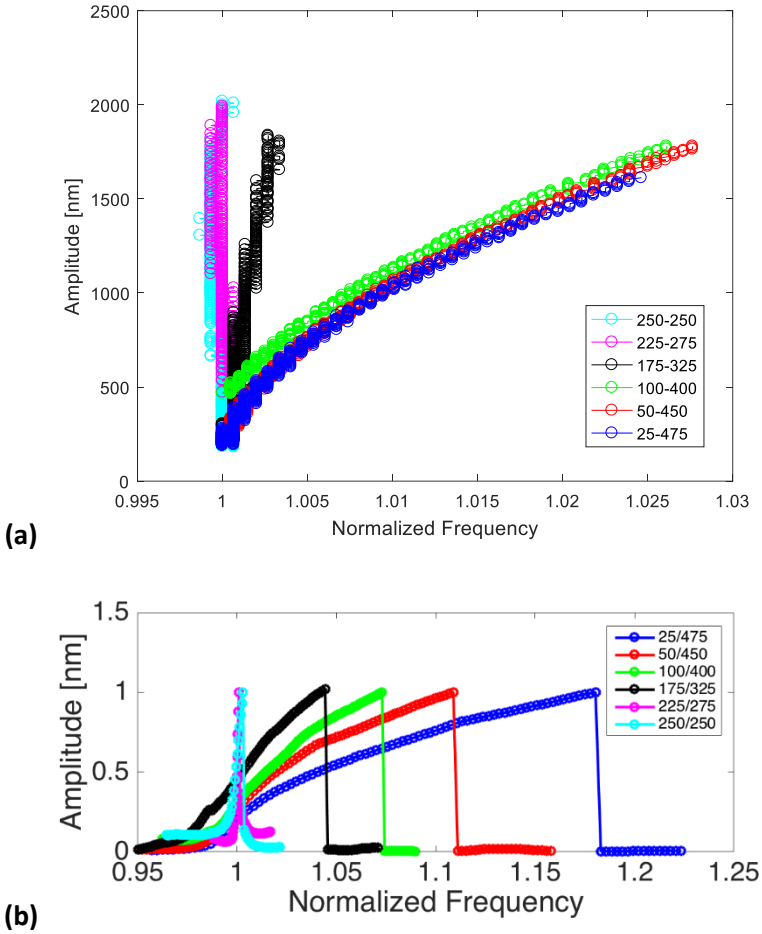

Figure 19: (a) Simulated backbone curves for different configurations of double cantilever structures released at first mode. (b) Experimentally obtained frequency responses of different configurations of double cantilever at first mode in the sweep-up direction.

3.2.3 Design Criteria

Two design criteria, i.e. physical location and thickness profile of the polymer component, are obtained for double cantilever structure. Figure 19a shows the simulated backbone curves when the polymer component is located at different positions along the *z*-direction; the level of nonlinearity diminishes as the polymer component gets closer to the middle of the structure. In Fig. 20, backbone curves are generated based on simulated results when different thicknesses of the

polymer component are employed; the global dynamics switches from nonlinear hardening to softening when there is an increase in the thickness of the polymer component. Therefore, desired nonlinear behaviors can be obtained by controlling the thickness of the polymer component. Note that the stiffness of the polymer component and the level of structural asymmetry both increases when thicker polymer component is employed; nonlinear softening behavior induced by structural asymmetry dominates over the nonlinear hardening behavior resulted from the increasing stiffness.

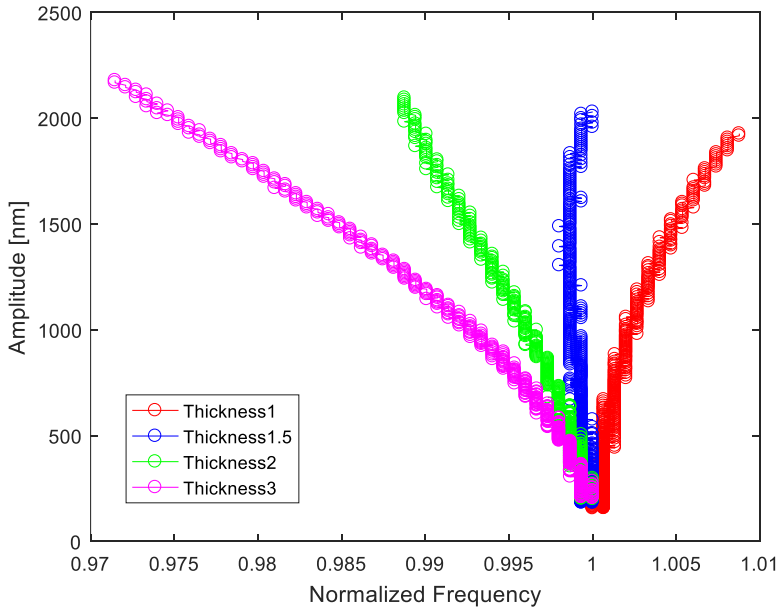

Figure 20: Simulated backbone curves for different thickness of the polymer component.

3.2.4 Field Output Results – Axial Strain Responses

In Fig. 19a, the global dynamics of the system switches from nonlinear hardening to linear resonance as the polymer component gets closer to the middle of the structure. To understand the reason behind this phenomenon, the axial strain responses of the two extreme configurations are investigated in Table 5. When the structure is initially oscillating at large amplitude and the polymer component is located at the end of the structure, the averaged values of axial strain (in red) at the midplane of the polymer component are positive; when the polymer component is

located at the middle of the structure, the averaged values of axial strain (in red) become zero throughout the simulation. The averaged values of axial strain (in red) at the midplane of the silicon component are all very close to zero no matter where the polymer component is located. Therefore, as the polymer component moves toward the middle of the structure, the polymer component becomes less stretched during oscillation and thus the level of nonlinearity diminishes within the system.

Table 5: Axial Strain Responses (blue) and averaged values (red) obtained at the midplanes of polymer and silicon components.

Configuration (LengthA_LengthB)	Strain response at the midplane of the polymer component	Strain response at the midplane of the silicon component
25_475 (polymer component is located at the end of the structure)	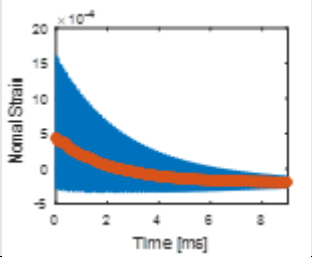	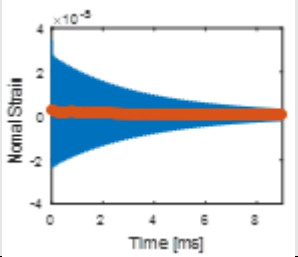
250_250 (polymer component is located at the middle of the structure)	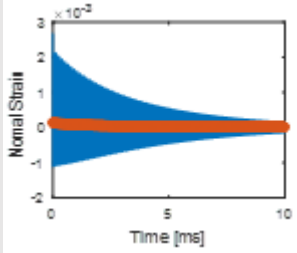	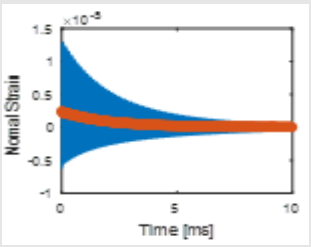

Chapter 4: Conclusion

4.1 Summary

In this research, the proposed FEA methodology is verified with experimental results and it is used to validate analytical assumptions. The global dynamics of single and double cantilever structures are characterized using FEA. Design criteria are established for both types of structures to calculate the targeted level of nonlinearity; these design criteria can be used to further develop tunable nonlinear micro-resonators with desired nonlinear behaviors.

Based on simulated backbone curves obtained from dynamic response of single cantilever-polymer structure, strong nonlinearity is presented when the structure is released at its first three flexural modes. The stretching within the polymer component is determined to be the source of nonlinear hardening by investigating the axial strain responses within both polymer and silicon components. Higher stiffness of the nonlinear component switches the global dynamics from nonlinear hardening to softening; therefore, single cantilever-polymer structures with targeted level of nonlinearity can be designed according to this design criterion.

For double cantilever structures, the physical location and thickness profile of the polymer component are found to be determinative on the level of nonlinearity. Nonlinearity diminishes as the polymer component gets closer to the middle of the structure; the global dynamics switches from nonlinear hardening to softening as the thickness of the polymer component increases. These two design criteria can also be considered for creating double cantilever structures with desired nonlinear behaviors.

4.2 Future Work

In this research, we choose 3D solid as the base feature for all the FE models; however, we neglected the locking phenomenon during bending, which means the solid elements show stiffer bending behavior comparing to analytical models. In general, locking effect is stronger when the thickness of the solid elements is significantly smaller than the other dimensions. To solve this issue, shell model should be considered in the future so that more accurate results can be obtained more efficiently.

During the preliminary stage of this research, the internal resonance of micromechanical resonators is observed experimentally on single cantilever structures. However, this research fails

to obtain the design criteria that triggers the internal resonance. Therefore, further investigation can also focus on internal resonance using FEA.

Reference

1. J. Rhoads, S. Shaw, K. Turner, "Nonlinear Dynamics and Its Applications in Micro- and Nanoresonators," 2010.
2. M. Lutz, A. Partridge, P. Gupta, N. Buchan, E. Klaassen, J. McDonald, K. Petersen, "MEMS Oscillators for High Volume Commerical Applications," 2007.
3. W. Zhang, K. Hu, Z. Peng, G. Meng, "Tunable Micro- and Nanomechanical Resonators," 2015.
4. K. Jensen, K. Kim, A. Zettl, "An atomic-resolution nanomechanical mass sensor," 2008.
5. B. Lassagne, D. Garcia-Sanchez, "Ultrasensitive Mass Sensing with a Nanotube Electromechanical Resonator," 2008.
6. N. Kacem, J. Arcamone, F. Perez-Murano, S. Hentz, "Dynamic range enhancement of nonlinear nanomechanical resonant cantilevers for highly sensitive NEMS gas/mass sensor applications," 2010.
7. H. Tilmans, W. Raedt, E. Beyne, "MEMS for wireless communications: 'from RF-MEMS components to RF-MEMS-SIP'," 2003
8. G.N. Nielson, D. Seneviratne, F. Lopez-Royo, P.T. Rakich, Y. Avrahami, M.R. Watts, H.A. Haus, H.L. Tuller, G. Barbastathis, "Integrated wavelength-selective optical MEMS switching using ring resonator filters," 2005.
9. L. Lin, C.T.-C. Nguyen, R.T. Howe, A.P. Pisano, "Microelectromechanical filters for signal processing," 1998.
10. H. Noh, S. Shim, M. Jung, Z. G. Khim, J. Kim, "A mechanical memory with a dc modulation of nonlinear resonance," 2010
11. A. Yao and T. Hikihara, "Logic-memory device of a mechanical resonator," 2014.
12. M. A. Hafiz, L. Kosuru, and M. I. Younis, "Microelectromechanical reprogrammable logic device," 2016.
13. H. Cho, M. Yu, A. F. Vakakis, L. A. Bergman, D. M. Mcfarland, "Tunable, Broadband Nonlinear Nanomechanical Resonator," 2010.
14. K. Asadi, J. Li, S. Peshin, J. Yeom, H. Cho, "Mechanism of geometric nonlinearity in a nonprismatic and heterogeneous microbeam resonator" 2017.
15. M. I. Younis, "MEMS Linear and Nonlinear Statics and Dynamics," 2011.
16. S.N. Mahmoodi, N. Jalili, M.F. Daqaq, "Modeling, Nonlinear Dynamics, and Identification of a Piezoelectrically Actuated Microcantilever Sensor," 2008.
17. L. Xu, Y. Liu, X. Fu, " Effects of the van der Waals Force on the Dynamics Performance for a Micro Resonant Pressure Sensor," 2016.
18. D. Antonio, D. H. Zanette, D. Lopez, "Frequency stabilization in nonlinear micromechanical oscillators," 2012.
19. R. B. Karabalin, R. Lifshitz, M. C. Cross, S. C. Masmanidis, M. L. Roukes, "Signal Amplification by Sensitive Control of Bifurcation Topology," 2011.
20. M. Kwon, W. H. Steier, "Microring-resonator-based sensor measuring both the concentration and temperature of a solution," 2008.

21. A. Pyayt, X. Zhang, J. Luo, A. Jen, L. Dalton, A. Chen, “Optical micro-resonator chemical sensor,” 2007.
22. D. Chen, J. Zhao, Y. Wang, J. Xie, “An electrostatic charge sensor based on micro resonator with sensing scheme of effective stiffness perturbation,” 2017.
23. B. Abdo, E. Arbel-Segev, O. Shtempluck, E. Buks, “Observation of Bifurcations and Hysteresis in Nonlinear NbN superconducting Microwave Resonators,” 2006.
24. L. G. Villanueva, E. Kenig, R. B. Karabalin, M. H. Matheny, Ron Lifshitz, M. C. Cross, M. L. Roukes, “Surpassing Fundamental Limits of Oscillators Using Nonlinear Resonators,” 2013.
25. J. N. Reddy, “Introduction to the Finite Element Method,” 2006.

Appendix

```
T = (t(end)-t(1))/length(t); % Sample time
Fs = 1/T;                    % Sampling frequency
L = length(t);

figure(1)
% subplot(2,1,1)
% plot(t,x)
% title('Mode 2')
NFFT = 2^nextpow2(L); % Next power of 2 from length of y
Y = fft(x,NFFT)/L;
f = (Fs/2000)*linspace(0,1,NFFT/2+1);
% f=f1/1000;

% Plot single-sided amplitude spectrum.
% subplot(2,1,2)

plot(f,2*abs(Y(1:NFFT/2+1)),'r')
xlim([0 max(f)/5])
xlabel('Frequency (kHz)')
ylabel('FFT Magnitude')
set(gca,'yscale','log')
```

Figure 21: MATLAB code for generating FFT plots.

```
%% Load Data
dt=t(end)/length(t);

x_part = x(1:500);
%% Wavelet Transform
    No_Freq = 3000;
    IniFreq = 1; FinFreq =1000000; % in Hz
    SampleFreq = 1/dt;
    F0 = 5; % From experience

[wt.tnew,wt.Freq,wt.Module]=freq_inst_morlet(x,SampleFreq,IniFreq,FinFreq,No_
Freq,F0);
    [m,n] = size(wt.Module);

[wt.tnew_twd,wt.Freq_twd,wt.Module_twd]=freq_inst_morlet(x,SampleFreq,IniFreq
,FinFreq,No_Freq,F0);
    [m_twd,n_twd] = size(wt.Module_twd);



%     figure(14)
%     subplot(3,1,1)
%     plot(T*10^6,x,'b-')
%     %xlim([0 300]);
%     xlabel('Time [\mus]');ylabel('Time response [a.u.]');
%
%
%     subplot(3,1,2)
%
```

```
%    semilogy(linspace(0,1,T(p)*fs/2)*fs/2,abs(y(1:T(p)*fs/2)),'r')
%
%     xlabel('frequency');ylabel('FFT Amplitude');
%
%
%    subplot(3,1,3)
    colormap(pink); MAP=colormap;
    colormap(ones(size(MAP))-MAP)
    imagesc(wt.tnew*10^3,wt.Freq/10^3,(wt.Module'.^0.4))
    %contourf(tnew1,Freq1*2*pi,Module1'.^1,'Edgecolor','None'), hold on
    xlabel('Time [ms]'); ylabel('Frequency [kHz]');
    set(gca,'YDir','normal');ylim([0 500]);
%     figure(2)
%     plot(t,x)
%     xlabel('Time [s]'); ylabel('Amplitude [\mum]');   ylim([-3
3]);set(gca,'YTick',[-3:3:3]);
 set(gca, 'FontName', 'Arial', 'FontSize', 20)

    %xlim=([0 4]);
    %set(gca,'XTick',[0:2:4]);
    %set(gca,'XTickLabel',0:2:4)
set(gca,'YTick',[0:50:500]);
    x0=10;
y0=10;
width=650;
height=500;
set(gcf,'units','points','position',[x0,y0,width,height])
```

Figure 22: MATLAB code for generating WT plots.

```
%% Signal Filter
N=length(t);
ts=t(end)/N;
fs = 1/ts;
%ts = 1/fs;
fc = 54000;
bs = (fc+6000);
bp = (fc-6000);
delta = 4000;
h = firls(350,[0,(bp-
delta)*2/fs,bp*2/fs,bs*2/fs,(bs+delta)*2/fs,1],[0,0,1,1,0,0]);
fvtool(h,1);figure;
filtered_x = filter(h,1,x);
plottf(x,ts);figure;
plottf(filtered_x,ts)
```

Figure 23:Signal Filter is developed for filtering undesired modes obtained from dynamic responses.

```
%% Backbone Curve & Nonlinear Coef.
clear q t1 w1 w2 tt p q2;
[q,locs] = findpeaks(filtered_x,'MinPeakDistance',14,'MinPeakHeight',0);

b=0;
bb=0;
dt=t(end)/length(t);

for i=1:length(locs)
    t1(i)=locs(i)*dt;
```

```
    q(i)=q(i)*1e3;
end
r=length(q);
% c=0;x=x
% for j=4:5:r-5
%     c=c+1;
%     w1(c)=1/(t(j+1)-t(j));
%     q2(c)=(q(j)+q(j+1))/2;
% end
kk=1;
kkk=15;    % Number of successive averaging periods
rr=floor((r-1)/kk);
for p=1:kk:r-kkk
    l=ceil(p/kk);
    tt(l)=(t1(p+kkk)-t1(p))/kkk;
    w2(l)=(1/tt(l))*0.001;
    q2(l)=(q(p)+q(p+kkk))/2;
    %q2(l)=((q(p)-qq(p))/2+(q(p+kkk)-qq(p+kkk))/2)/2;
end
% ee=length(w2);
% subplot(2,1,1)
% plot(w2,q2,'o-')
% %plot(w1,q(1:ee),'o-')
% title('Nonlinear frequency response')
% subplot(2,1,2)
% plot(t(1:ee),w2,'o-')
% title('Resonance Frequency-Time')
%
%
% kk=1;
% kkk=10;    % Number of successive averagigng periods
% rr=floor((r-1)/kk);
% for p=1:kk:r-kkk
%     l=ceil(p/kk);
%     tt(l)=(t(p+kkk)-t(p))/kkk;
%     w2(l)=(1/tt(l))*0.001;
% end
e=length(w2);
% figure(2)
% subplot(2,1,1)
% plot(w2,q(1:e),'o-')
% title('Nonlinear frequency response')
% subplot(2,1,2)
% plot(t(1:e),w2,'o-')
% title('Resonance Frequency-Time')


modelFun = @(a,x) (24/a(1) .* (x./a(2) -1) ).^0.5;  % a(1) =9*alpha3-
10*alpha2^2, a(2) = fo, x is frequency, a(1)
%modelFun = @(a,x) (24/a(1) .* (x.^2./a(2).^2 -1) ).^0.5;  % a(1) =9*alpha3-
10*alpha2^2, a(2) = fo, x is frequency, a(1)

%startingVals = [-1 105];
%startingVals = [-1 103];
startingVals = [0.01 w2(length(w2)-2)];
```

```
z=5;   % To eliminate the scattered points.
w3=w2(z:e);
q3=q2(z:e);
options = statset('MaxIter', 10e7, 'TolFun', 10e-10, 'TolX', 10e-10);
%coefEsts = nlinfit(Freq_max(1:3), Amp_max(1:3), modelFun, startingVals,
options);
%coefEsts = nlinfit(Freq_max(4:6), Amp_max(4:6), modelFun, startingVals,
options);
coefEsts = nlinfit(w3,q3, modelFun, startingVals, options);

format long
mu=real(coefEsts(1))
xgrid = linspace(coefEsts(2), max(w2), 1000);
%xgrid = linspace(min(w2), coefEsts(2), 1000);
%xgrid = linspace(min(Freq_max-2), coefEsts(2),  1000);
%xgrid = linspace(100,108,  1000);

figure()
plot(w3,q3,'ro-')
hold on
line( xgrid, real(modelFun(coefEsts, xgrid)), 'Color', 'b', 'LineWidth',2);
iw3= w3';
iq3= q3';
% xlim([Freq_max(length(frames))-5 Freq_max(length(frames))+5])
%
% ylim([5 max(q)*1.1])
format long
mu=real(coefEsts(1));

xlabel ('Frequency [kHz]')
ylim([0 max(q2)]);
ylabel ('Amplitude [nm]')
set(gca, 'FontName', 'Arial', 'FontSize', 16)

% title
({'NonlinearCoefficient=',num2str(mu)},'FontSize',14,'FontName','FixedWidth')
;
```

Figure 24:MATLAB code for generating backbone curves and nonlinear coefficients.